Sustainable Polymers Derived From Glucose and Fructose

Derek J. Saxon
Senior Thesis, Spring 2015
Department of Chemistry
Ripon College

INTRODUCTION

Plastic waste is generated in excess of 30 million tons each year in the United States, with only thirteen percent recovered for recycling. This is not only an issue faced by the United States; rather, it is a global concern that must be addressed within the next 20 years. While many European countries are exploring alternate methods to recycle plastic waste, the long-term solution lies in the development of a new generation of materials. To accomplish this feat, scientists must move away from the petroleum feedstock currently used and develop sustainable polymers from natural feedstocks, such as biomass. This will also open up new possibilities for applications in biomedical devices.

Commercial polymers are derived from fossil fuels and produced on a teragram scale annually.[1] Polymers have proven their usefulness in a wide range of applications including plastics bottles, packaging, fibers, adhesives, toys, and biomedical devices. They also offer an array of valuable characteristics such as being durable, chemically resistant, conductive, elastic, lightweight, and self-healing.[1] While petro-polymers are convenient and have well-defined properties, their practicality is offset by a discernible lack of sustainability. Petro-polymers are derived from a non-renewable feedstock, rapidly depleting these valuable resources, and are too infrequently recovered for utilization in other materials causing them to accumulate in landfills at alarming rates.[1] Landfills accrue over 30 million tons of plastic waste per year on average, composing approximately 12.7% of all generated solid waste.[2] The trends of current polymeric materials cannot be sustained and practices for the manufacture and disposal of polymers must be altered tremendously.

A new generation of polymers derived from renewable feedstocks is vital to creating a world with sustainable materials. These sustainable polymers must have a low production cost as well as properties that are competitive with the performance of current polymers.[1] Carbohydrates are inexpensive, produced on a scale of 10^7 metric tons annually and biomass recoverable, making them a viable source for the development of renewable materials.[3] Carbohydrates are also the building blocks of many naturally occurring polymers, including the most abundant, cellulose. Cellulose and other modified polysaccharides have recently been employed for numerous applications including drug delivery, clothing, food,

adhesives, paint, and flat screen displays.[4,5] An interesting approach to produce polysaccharides with desirable properties is through the assembly of carbohydrates into polymers via chemical means, attempting to mimic the work of nature.

One approach for the modification of cellulose and the polymerization of carbohydrates is through the use of ionic liquids (ILs). Cellulose dissolution traditionally requires harsh conditions and expensive solvents that are not recoverable. ILs are organic salts, known as "designer solvents", with melting points below 100 ºC; they have unique properties, determined by the structure of the cation and anion, such as high thermal stability and negligible vapor pressure.[6] ILs are able to tolerate a variety of reactants and allow for the synthesis of many derivatives of cellulose.[5] Imidazolium-based ILs show the greatest promise in this area because of their ability to solvate cellulosic polysaccharides as well as simple carbohydrates.[6] This method of building carbohydrate polymers involves the use of step-growth polymerization techniques, in which a small molecule is extruded during the course of the reaction (Scheme 1). Step-growth polymerization is difficult to control and generally produces polymers of low molecular weight and wide polydispersity, not ideal for many industrial applications.

Scheme 1. General step-growth polymerization of a diacid and diol through the extrusion of water.

Another approach for the production of renewable polymers from carbohydrates is through the ring-opening polymerization (ROP) of cyclic esters, or lactones. Many lactones can be produced from carbohydrate starting materials, opening the door to countless possibilities. It is feasible to initiate ROP through a variety of metal and organic catalysts, producing aliphatic polyesters with attractive characteristics.[1,7,8] Many examples of ROP are presented in the literature, including sustainable polymers and copolymers of lactide, glycolide, ε-caprolactone and menthide (Scheme 2).[1,8–13] Furthermore, ROP is a form of chain-growth polymerization, capable of exceptional molecular weight, polydispersity and stereochemical control.[1] The physical properties of aliphatic polyesters produced from the ROP of

lactones can also be controlled, broadening the spectrum of potential applications.[7]

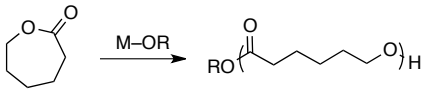

Scheme 2. Ring-opening polymerization of ε-caprolactone initiated by a metal alkoxide.

One of the simplest forms of a carbohydrate-based lactone is gluconolactone (GL), produced from glucose. Glucose is produced worldwide on a larger scale and at a lower cost than other common monomers and can be easily converted to GL by an enzymatic process (Scheme 5).[9,10] For example, 2.1 million metric tons of methyl methacrylate is produced annually at a cost of \$1.32 kg^{-1} whereas 5 million metric tons of glucose is produced annually at a cost of \$0.76 kg^{-1}.[10] Moreover, GL is biocompatible and frequently used as a food additive, making it a promising candidate for biomedical and sustainable applications.[7–9] This study focuses on the development of sustainable polymers derived from a biomass feedstock, primarily glucose and fructose, as well as the mechanism of ROP.

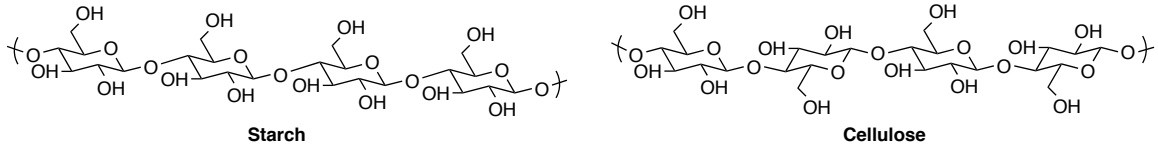

Figure 1. Structure of starch and cellulose showing α- and β-linkages of glucose monomers, respectively. The β-linkages of cellulose are characterized by glucose molecules that are rotated 180º to one another.

To investigate the step-growth polymerization of carbohydrates in an IL media, glucose and fructose were subjected to condensation polymerization. This approach was employed because molecules of either carbohydrate can be linked together through α- or β-linkages as in starch and cellulose, removing water as the reaction progresses (Figure 1). Condensation polymerization is an equilibrium process due to the extrusion of water during the reaction; thus, removal of water from the reaction mixture is vital to the progress of the reaction.[14] Two common techniques utilized for this are the entrapment of formed water via a Dean–Stark trap or by passing a continuous stream of nitrogen gas through the reaction flask. Two imidazolium-based ILs were studied as potential solvents for this type of polymerization: 1-ethyl-3-

methylimidazolium chloride, [emim][Cl], and 1-butyl-3-methylimidazolium chloride, [bmim][Cl] (Figure 2). These ILs were chosen due to their capability to dissolve both glucose and fructose, and likely the formed poly(glucose) and poly(fructose), as well as for their low-cost as compared to other known ILs of similar ability.[6,15] Additionally, metaboric acid and titanium butoxide [Ti(O*n*-Bu)$_4$] were examined for their reported abilities to initiate condensation polymerization of glucose and lactic acid, respectively.[14,16]

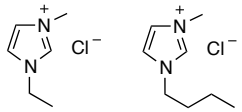

Figure 2. Structure of [emim][Cl] and [bmim][Cl], the ILs used for condensation polymerization of glucose and fructose.

To explore the ROP of the glucose-derived monomer, GL was prepared[17] and subjected to three metal complexes – titanium butoxide [Ti(O*n*-Bu)$_4$], aluminum isopropoxide [Al(O*i*-Pr)$_3$] and zinc stearate [Zn(St)$_2$] – because metal alkoxides and carboxylates are effective ROP initiators (Figure 3).[8,11] Each metal complex was successfully employed, but Al(O*i*-Pr)$_3$ was selected for a comprehensive study due to its enhanced Lewis acidity and minimal toxicity.[12,13] Reaction times and temperatures were varied to determine optimum conditions for PGL formation. Reactions were quenched after 1, 4, 8, or 24 h and the temperatures studied were room temperature, 40 ºC, and 70 ºC. Temperatures over 100 ºC were not scrutinized because GL is a sensitive molecule and would likely decompose at high temperatures. Moreover, Al(O*i*-Pr)$_3$ is known to be active at low temperatures, minimizing the amount of potential side reactions caused by high temperatures.[7] Since GL and PGL have limited solubility in solvents other than water, they pose a challenge for conducting polymerizations and purification of products. To combat this issue, GL was acetylated to form AGL, a monomer possessing characteristics that make it easy to handle and purify (Scheme 5).[18] Furthermore, additional optimization experiments are unnecessary because AGL can be polymerized under similar conditions as GL to produce PAGL. After PAGL is isolated, PGL can be generated by straightforward removal of the protecting groups.

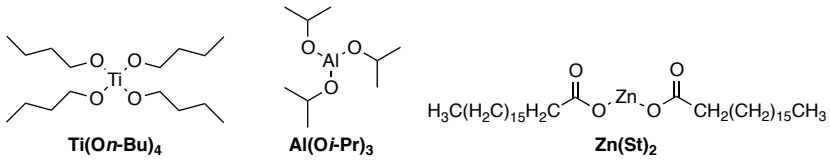

Figure 3. Structures of Ti(O*n*-Bu)$_4$, Al(O*i*-Pr)$_3$ and Zn(St)$_2$, the organometallic initiators used for the ROP of GL and AGL.

Since lactones are abundant and readily available, ROP will be a heavily employed method in the development of biorenewable polymers. Thus, it is vital to understand the mechanism by which polymers are formed with various initiators in order to improve the design and production of competitive sustainable polymers. Consequently, three potential mechanisms of GL polymerization initiated by Al(O*i*-Pr)$_3$ were investigated computationally: anionic 1, anionic 2 and coordination-insertion (Scheme 6).[7,8,11–13,19] Anionic 1 and anionic 2 involve the nucleophilic attack of GL by an isopropoxide ligand, resulting in acyl-oxygen and alkyl-oxygen cleavage of GL, respectively. This causes an alkoxide propagating species for the anionic 1 pathway and a carboxylate propagating species for the anionic 2 pathway. Coordination-insertion also produces the alkoxide propagating species, but goes through a 4-atom coordination before the breaking or formation of bonds. Moreover, structure and reactivity of the Al(O*i*-Pr)$_3$ monomer (A_1), dimer (A_2), trimer (A_3) and tetramer (A_4) were studied in detail (Figure 16). Aluminum-based organometallics are known to aggregate in solution and A_3 has previously been proposed to be more reactive towards ROP.[7] Herein, the synthesis and characterization of sustainable polymers derived from glucose and fructose is reported along with the mechanism of Al(O*i*-Pr)$_3$ initiated ROP.

EXPERIMENTAL

Unless otherwise noted, all chemicals were purchased from Sigma–Aldrich and used without further purification. Ti(O*n*-Bu)$_4$, GL and AGL were synthesized according to previously reported procedures for preliminary studies and GL was later purchased for further investigation.

Characterization

^{1}H and ^{13}C NMR spectroscopy was performed on a Varian MERCURY-300. FT-IR was performed on a PerkinElmer Spectrum 100 spectrometer. GC/MS was performed using a Hewlett-Packard 5890 Series II GC and 5971 Series MS. High-resolution LC/MS was performed using an Agilent Technologies 1260 Infinity LC and 6230 TOF MS.

Experimental Methods

Ti(O*n*-Bu)$_4$. Ti(O*i*-Pr)$_4$ (10.0 mL, 35.18 mmol) was refluxed with excess *n*-butanol (100 mL) for 26 h. The resulting mixture was distilled to collect Ti(O*n*-Bu)$_4$ (8.1644 mL, 23.94 mmol, 70.9%) and subsequently rotovapped to remove excess butanol. ^{1}H NMR (300 MHz, $CDCl_3$): δ 4.3 (s, 2H, isopropanol), 3.7 (t, 2H), 1.7-1.2 (m, 4H), 0.92 (t, 3H); FT-IR ($CDCl_3$): 3624, 2959, 2933, 2873, 1464, 1365, 1126, 1087, 1037, 969 and 865 cm^{-1}.

Poly(glucose) and Poly(fructose). A sample procedure is as follows: fructose (2.0 g, 11.101 mmol) and either metaboric acid (21.5 mol%, 0.1048 g, 2.392 mmol) or Ti(O*n*-Bu)$_4$ (3.18 mol%, 0.12 mL, 0.353 mmol) were dissolved in [bmim][Cl] (20 mL) in a 3-necked round bottom flask. Nitrogen was passed through the heated flask (60 °C) for 30 h. Aliquots were removed from the mixture after 1, 8 and 22 h and products were precipitated with water to monitor reaction progress. FT-IR (KBr pellet): 3416, 3083, 1621, 1594 cm^{-1}.

GL. Silver carbonate on celite (2.0070 g) was prepared from Ag_2CO_3 (1.0067 g, 3.651 mmol) and celite (2.0003 g) and subsequently refluxed with glucose (0.0700 g, 0.3885 mmol) in benzene (40 mL) for 1 h. The Ag_2CO_3/celite solid was removed via filtration and washed with hot benzene; the solvent was removed by rotary evaporation and GL was collected as a colorless solid (23%). GC/LR EI-MS: t_R 8.069 min; *m/z* 177 [$M^{+\bullet}$-$H^{\bullet}$], 145 [$M^{+\bullet}$-$CH_2OH^{\bullet}$], 133 [$M^{+\bullet}$-$CO_2^{\bullet}$] and 91 [$M^{+\bullet}$-$(CH)_3(OH)_3^{\bullet}$].

PGL. A sample procedure is as follows: GL (0.2635 g, 1.47917 mmol), DMF (1.40 mL) and Al(O*i*-Pr)$_3$ (1.15 mol%, 3.5 mg, 0.0171367 mmol) were combined in a 4 dram round-bottom vial. The headspace was purged with N_2 and sealed with a PTFE-lined cap. The mixture was stirred for 8 h at room

temperature. The reaction was quenched with 3M HCl and PGL was precipitated with excess ethyl acetate. ^{1}H NMR (300 MHz, D_2O): δ 4.42 (m, 1H, endgroup CH), 3.95 (m, 2H), 3.61 (m, 4H), 2.76 (s, 1H), 2.60 (s, 6H, endgroup CH_3); ^{13}C NMR (300 MHz, D_2O): δ 173.4, 81.1, 72.3, 70.5, 66.6, 59.6, 18.2 (endgroup CH_3); FT-IR (KBr pellet): 3469, 3278, 2967, 2930, 2908, 2431 and 1729 cm^{-1}.

AGL. A sample procedure is as follows: GL (2.0898 g, 11.7312 mmol) was added to a stirred solution of Ac_2O (10.6 mL) and $ZnCl_2$ (1.0100 g, 7.4101 mmol). After 2 h the reaction mixture was poured onto crushed ice (10 g) and stirred for 30 min. The resulting solution was extracted with ethyl acetate (3 x 5 mL) and the organic layer was washed successively with saturated $NaHCO_3$ (5 mL), saturated NaCl (5 mL) and dried over $MgSO_4$. The filtered solution was concentrated by rotary evaporation to yield a yellow liquid (92%). ^{1}H NMR (300 MHz, $CDCl_3$): δ 5.55 (t, 1H), 5.36 (t, 1H), 5.10 (d, 1H), 4.62 (m, 1H), 4.37 (q, 1H), 4.27 (d, 1H), 4.22 (d, 1H), 4.11 (q, 1H), 2.21 (s, 3H, CH_3), 2.15 (s, 3H, CH_3), 2.08 (m, OAc), 1.24 (t, 2H, H_2O); ^{13}C NMR (300 MHz, $CDCl_3$): δ 171.0, 170.5, 170.3, 169.9, 166.4, 76.6, 70.3, 66.3, 61.2, 22.1, 20.7, 20.5, 20.4, 20.3 (OAc); FT-IR ($CDCl_3$): 2989, 2942, 2683, 2632, 2561, 2116, 1826, 1765, 1430 and 1370 cm^{-1}.

PAGL. A sample procedure is as follows: AGL (0.50 mL, 1.4438 mmol), THF (1.46 mL) and Al(O*i*-Pr)$_3$ (1.12 mol%, 3.3 mg, 0.01615 mmol) were combined in a 2-dram vial. The headspace was purged with N_2 and sealed with a PTFE-lined cap. The mixture was stirred for 48 h at room temperature with aliquots removed after 1, 3, 5, 7 and 24 h. The reaction was quenched with 3M HCl and PAGL was precipitated with excess methanol. ^{1}H NMR (300 MHz, $CDCl_3$): δ 6.45 (d, 1H), 5.62 (q, 1H), 4.84 (s, 1H), 4.77 (q, 2H), 4.36 (m, 3H), 3.76 (m, 1H, endgroup CH), 2.26 (d, OAc), 1.87 (s, 6H, engroup CH_3); ^{13}C NMR (300 MHz, $CDCl_3$): δ 228.1, 177.8, 170.5, 126.1, 109.1, 72.6, 64.1,61.9, 20.8; FT-IR (KBr pellet): 3390, 1765, 1696, 1377 cm^{-1}.

Theoretical Methods

All calculations were accomplished with the Gaussian 09 electronic structure program suite.[20] Gas-phase geometries were optimized using DFT calculations with the M06L functional[21] and the 6-31G(d) basis set.[22] All structures were characterized as local minima or transition states from computations of vibrational frequencies.[23] Single-point M06L calculations were included for the effects of DMF solvation with the SMD continuum solvation model.[24] Three potential mechanisms (anionic 1, anionic 2 and coordination-insertion) of GL ring-opening polymerization were investigated by computing thermodynamic data and creating a potential energy surface. Conformational analyses of GL and Al(O*i*-Pr)$_3$ were performed using Spartan 08 to thermodynamically determine lowest energy conformers at each point along the potential energy surface.[25] Structure and reactivity of A_1, A_2, A_3 and A_4 were examined by a model system initially and later by the ring-opening of GL.

RESULTS AND DISCUSSION

*Synthesis and Characterization of Ti(O*n*-Bu)$_4$ Initiator*

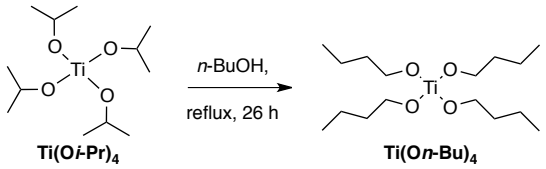

Scheme 3. Synthesis of Ti(O*n*-Bu)$_4$.

As shown in Scheme 3, Ti(O*n*-Bu)$_4$ was effectively prepared by reflux of Ti(O*i*-Pr)$_4$ with excess *n*-butanol. The actual yield is slightly higher because the presented yield does not include the isolated product obtained from the removal for ^{1}H NMR analysis. ^{1}H NMR spectroscopy shows the ligand exchange via formation of butoxide ligand peaks and loss of isopropoxide ligand peaks (Figure 4). Large solvent peaks are observed in the spectra due to abundance of butanol present in the solution; the peak at 4.3 ppm (Panel A) is most probably from residual butanol, disappearing after rotary evaporation (Panel B). Excess butanol was used in the reaction to drive the equilibrium towards Ti(O*n*-Bu)$_4$ formation. The

reaction was also monitored by ^{1}H NMR each hour for the first 7 h of reflux, revealing nearly full conversion after 5-6 h.

FT-IR analysis has provided more evidence about the structure and purity of the product, especially around the 3500–2700 cm^{-1} region (Figure 5). This region is key in distinguishing between the isopropoxide and butoxide ligands. Notably, the stretches around 900 and 800 cm^{-1} are due to the $CDCl_3$ solvent that was not removed from the spectrum when the background scan was acquired. The ^{1}H NMR and FT-IR spectra are in agreement with previous reports, providing confidence in the characterization of the product.

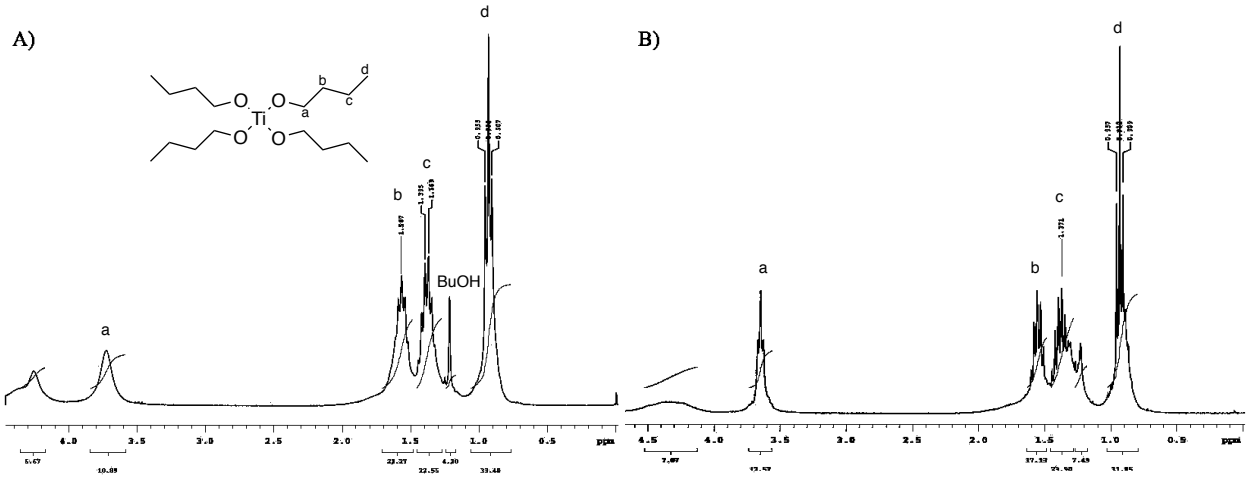

Figure 4. ^{1}H NMR spectra (300 MHz, $CDCl_3$) of Ti(O*n*-Bu)$_4$ after distillation (A) and after rotary evaporation to remove remaining butanol and isopropanol (B).

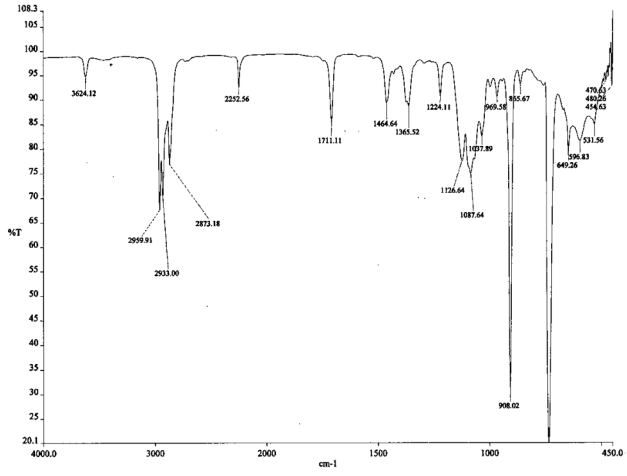

Figure 5. FT-IR spectrum ($CDCl_3$) of Ti(O*n*-Bu)$_4$ after rotary evaporation. The two large stretches around 900 and 800 cm^{-1} correspond to $CDCl_3$ that was not removed in the background scan.

Synthesis of Condensation Polymers

The polycondensation of glucose and fructose catalyzed by either metaboric acid or Ti(O*n*-Bu)$_4$ was attempted. The reactions were carried out in a renewable IL medium; products were precipitated with water and collected as a brown/yellow solid via centrifugation. The solid extract showed limited to no solubility in common organic solvents including $CHCl_3$, CH_3CN, DMSO and water; thus, NMR spectroscopy and mass spectrometry analyses were unable to be performed. FT-IR analysis shows alcohol functionality at 3416 cm^{-1} as well as C-H stretches near 3000 cm^{-1}, as expected. However, stretches at 1621 and 1594 cm^{-1} represent C=C and C-C stretches in a ring system (Figure 6). This double bond stretch suggests the degradation of glucose and fructose to furan-derived products, including 5-hydroxymethylfurfural (HMF), levulinic acid, humic acids and many other known side-products (Scheme 4).[26]

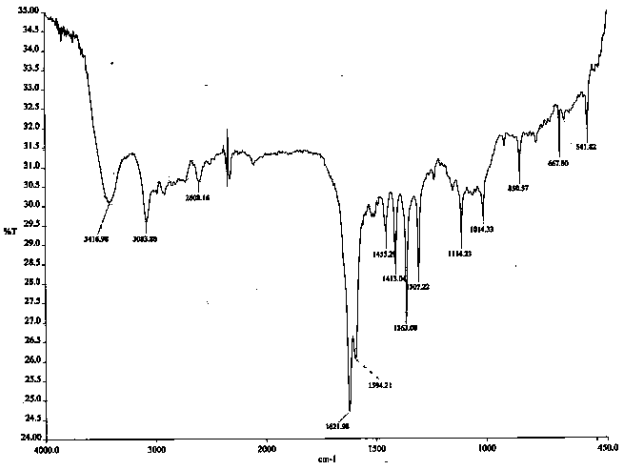

Figure 6. FT-IR spectrum (KBr pellet) of the uncharacterized solid product from glucose and fructose polycondensation. The peaks at 3416, 3083, 1621, 1594 cm^{-1} suggest the degradation to furan-derived products, such as HMF.

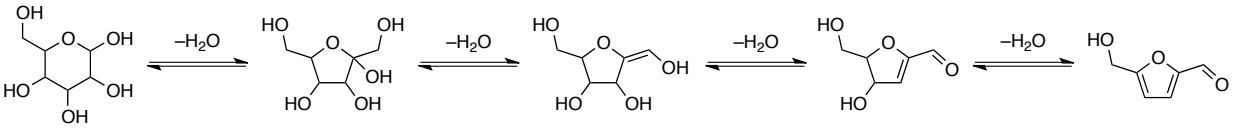

Scheme 4. Degradation of glucose and fructose to HMF via the removal of water.

Degradation is caused by the over-dehydration of glucose and fructose and is likely a result of the reaction conditions. Removal of water is crucial for condensation polymerization, which required elevated

temperatures; however, simple carbohydrates are sensitive and often decompose at their melting temperature. The observed degradation of glucose and fructose to HMF involves the formation of an aromatic furan ring as depicted in Scheme 4. Recent studies also suggest that ILs facilitate the conversion of glucose and fructose to HMF.[27] The role of the two catalysts in the degradation was investigated by reproducing the reaction conditions without the addition of a catalyst. This analysis revealed that neither catalyst played a role in the products obtained, further suggesting the degradation of glucose and fructose was due to high temperatures and ILs. It is noteworthy to mention that [bmim][Cl] was the preferred medium over [emim][Cl] for its solvent capability and ease of handling. Moreover, the ILs were easily recovered after precipitation of products through removal of water by distillation. Further investigation may be done to improve the IL recovery methodology for applications in large-scale reactions.

Synthesis of Monomers and Ring-Opened Polymers

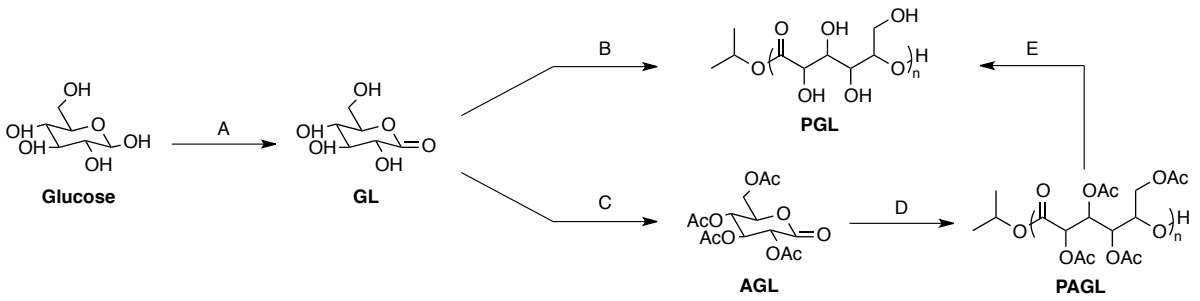

Scheme 5. Synthesis of GL, PGL, AGL and PAGL. Conditions: (A) Ag_2CO_3/celite, benzene, reflux, 1 h; (B) Al(O*i*-Pr)$_3$ (1 mol%), DMF, r.t., 8 h; (C) $ZnCl_2$, Ac_2O, r.t., 2 h; (D) Al(O*i*-Pr)$_3$ (1 mol%), bulk or THF, r.t., 48 h; (E) NaOH, MeOH, Δ.

As shown in Scheme 5, the anomeric carbon of glucose was oxidized by Ag_2CO_3 on celite to afford GL in modest yield (23%). The structure of GL was characterized by GC/MS, which exhibited four major fragments at 177, 145, 133 and 91 (t_R = 8.069 min), as shown in Figure 7.

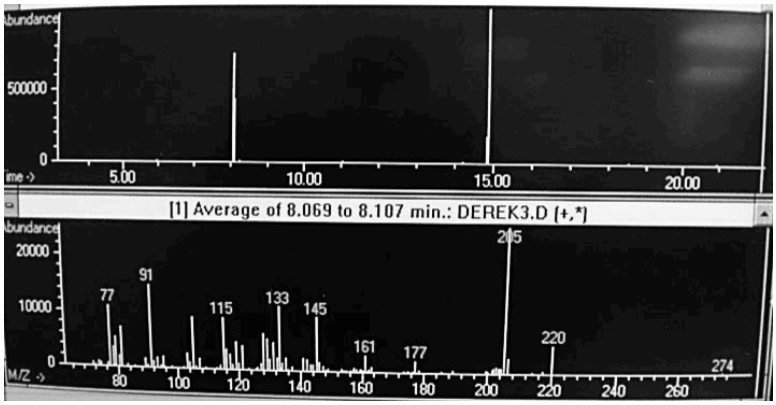

Figure 7. GC/LR EI-MS (t_R = 8.069 min) spectrum of GL.

GL was then homopolymerized to PGL using Al(O*i*-Pr)$_3$ as the initiator and DMF as the solvent. ^{1}H and ^{13}C NMR spectroscopy display the incorporation of terminal isopropyl group, supporting the formation of the ring-opened polymer (Figure 8). Integration shows the proportion of repeat units is much greater than terminal groups and gives a monomer conversion >90%, as expected for a chain-growth polymer. FT-IR spectroscopy exhibited the expected peaks (Figure 9). Polymerizations were studied at room temperature, 40 ºC and 70 ºC and quenched after 1, 4, 8 or 24 h. It was determined by NMR that polymerizations carried out for 24 h at room temperature produced the best results. By ^{1}H NMR endgroup analysis, PGL was found to have an M_w = 10,500; an M_n = 7,200 was determined by LC/ESI-TOF MS and the PDI was calculated to be 1.45. GL and PGL are only sparingly soluble in solvents other than water, making them difficult to work with under normal conditions; thus, another route for sustainable polymer synthesis was employed.

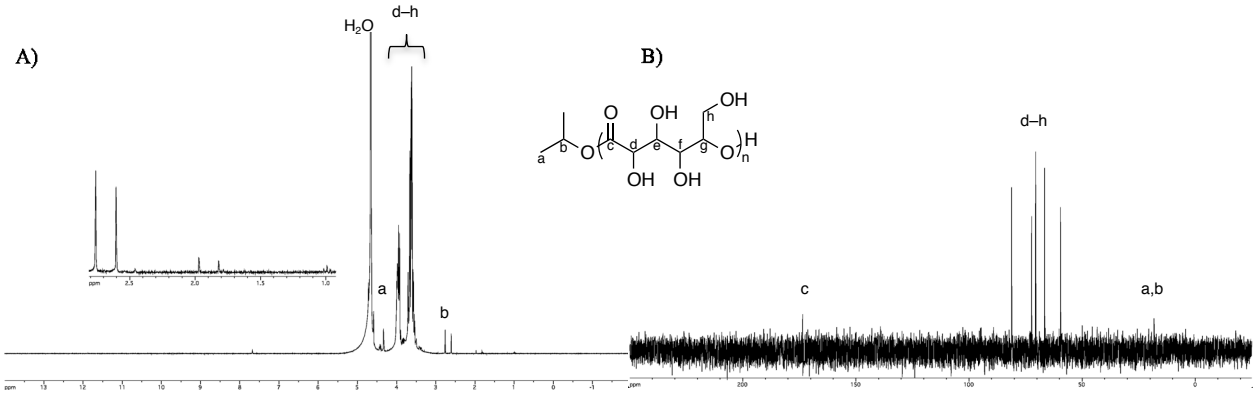

Figure 8. (A) ^{1}H and (B) ^{13}C NMR spectrum (300 MHz, D_2O) of PGL.

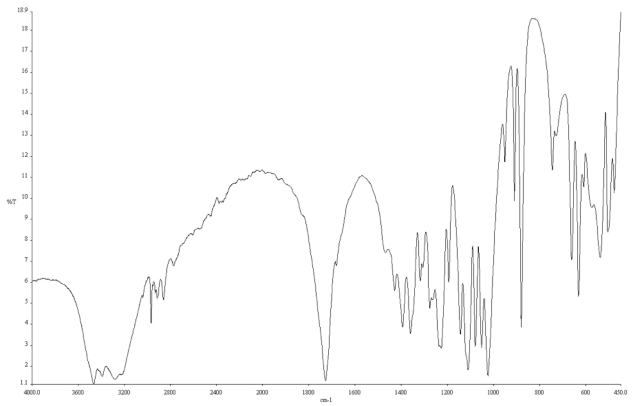

Figure 9. FT-IR spectrum (KBr pellet) of PGL.

AGL was prepared in high yield by acetylation of GL with $ZnCl_2$ and Ac_2O (92%). ^{1}H and ^{13}C NMR spectroscopy verified the protection of the four alcohols of GL (Figure 10). FT-IR also shows the incorporation of new C=O and C-H stretches from the protecting groups (Figure 11).

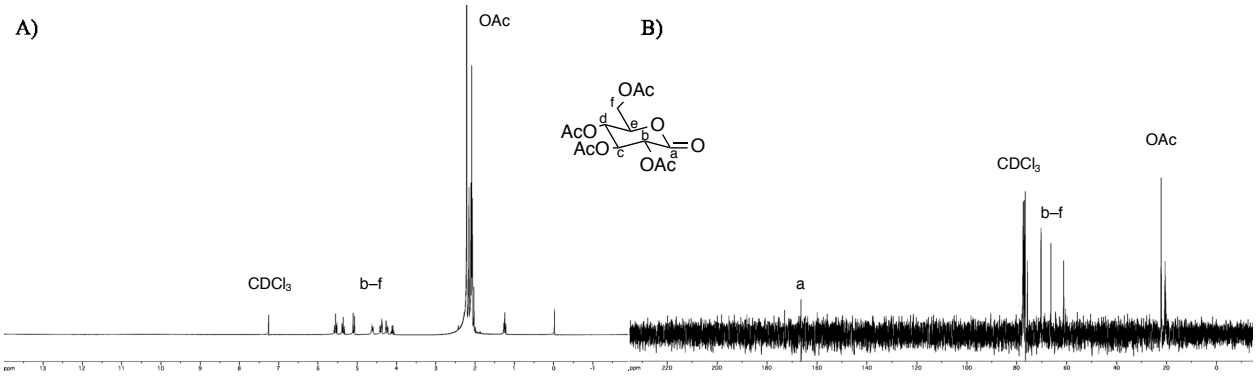

Figure 10. (A) ^{1}H and (B) ^{13}C NMR spectrum (300 MHz, $CDCl_3$) of AGL.

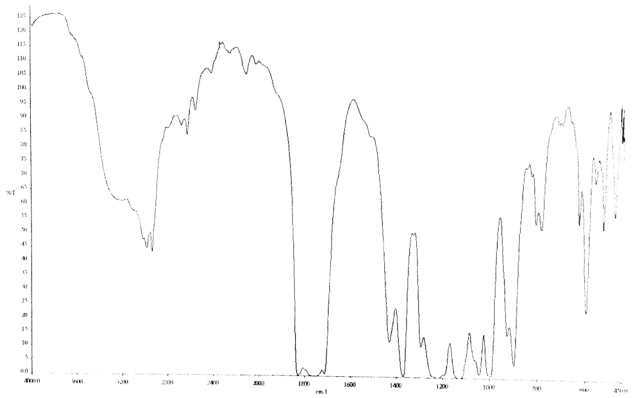

Figure 11. FT-IR spectrum ($CDCl_3$) of AGL.

AGL was subsequently homopolymerized to PAGL with Al(O*i*-Pr)$_3$ initiator in bulk or with THF as the solvent. Likewise, ^{1}H and ^{13}C NMR spectroscopy show in the incorporation of terminal isopropyl group, and integration again shows a monomer conversion >90% (Figure 12). FT-IR spectroscopy exhibits the expected broad stretches as well as two distinct carbonyl peaks for the backbone and acetyl groups (Figure 13). Polymerizations were studied at room temperature and quenched after 1, 3, 5, 7, 24 or 48 h. It was determined by NMR that polymerizations carried out for 48 h at room temperature produced the best results. PAGL was found to have an M_w = 85,000 by ^{1}H NMR endgroup analysis. Facile deprotection of PAGL with NaOH in methanol affords PGL in quantitative yield.

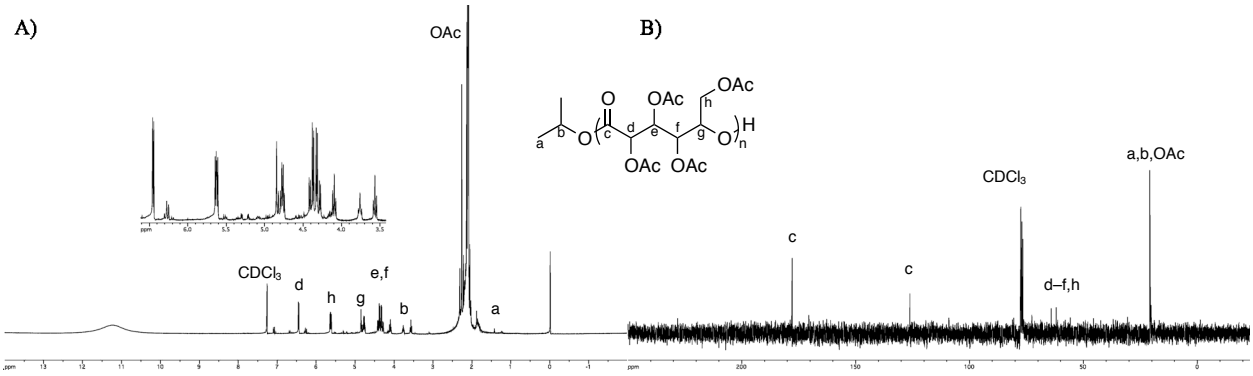

Figure 12. (A) ^{1}H and (B) ^{13}C NMR spectrum (300 MHz, $CDCl_3$) of PAGL.

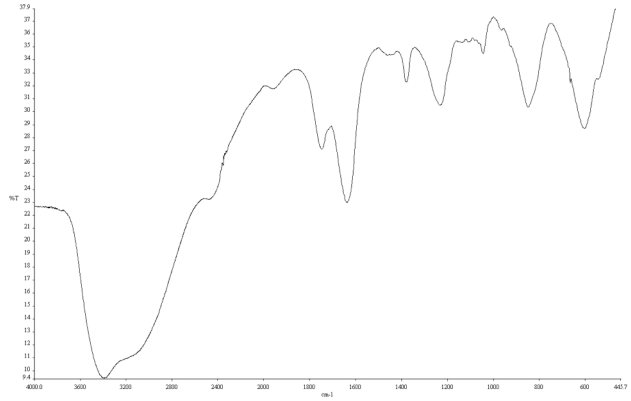

Figure 13. FT-IR spectrum (KBr pellet) of PAGL.

*Mechanism of Al(O*i*-Pr)$_3$ Initiator Toward ROP*

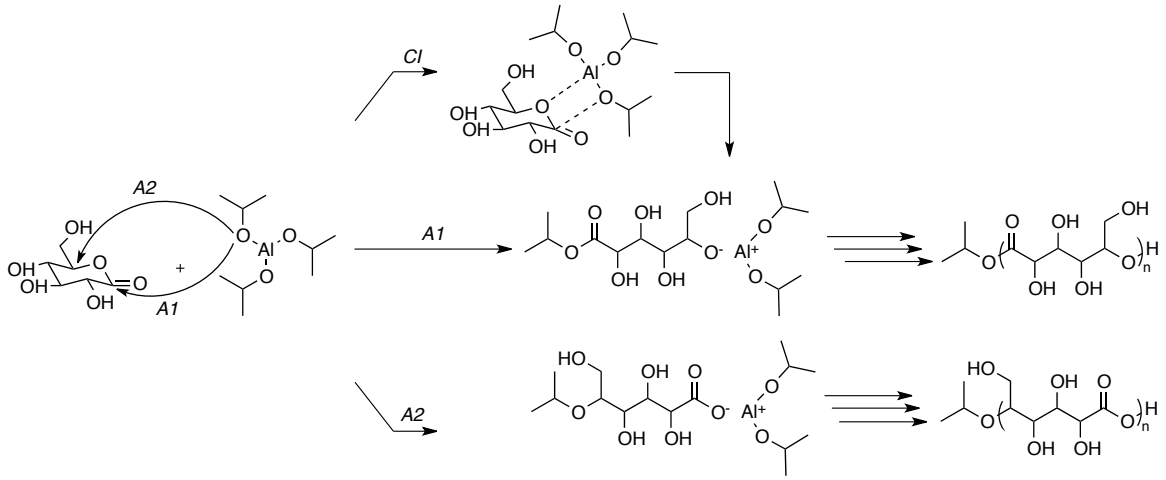

Scheme 6. Investigated pathways of GL polymerization initiated by Al(O*i*-Pr)$_3$ monomer, A_1. Anionic 1 involves the nucleophilic attack of the GL carbonyl by an isopropoxide ligand, resulting in acyl-oxygen cleavage and an alkoxide propagating species. Anionic 2 involves the nucleophilic attack of the GL C-5 by an isopropoxide ligand, resulting in alkyl-oxygen and a carboxylate propagating species. Coordination-insertion goes through a 4-atom coordination before cleaving the GL acyl-oxygen bond, which generates the same alkoxide propagating species as in anionic 1.

As shown in Scheme 6, three pathways were investigated for the ring-opening polymerization of GL initiated by the monomeric A_1 species. The anionic 1 pathway involves the nucleophilic attack of the GL carbonyl by an isopropoxide ligand, resulting in acyl-oxygen cleavage and an alkoxide propagating species. The GL alkoxide becomes the nucleophilic ligand, causing the polymer chain to grow. Termination of the polymerization with dilute acid results in an alcohol endgroup as well as the isopropyl endgroup from initiatior. The anionic 2 pathway consists of nucleophilic attack of the GL C-5 by an isopropoxide ligand, resulting in alkyl-oxygen and a carboxylate propagating species. Similarly, the GL carboxylate becomes nucelophilic, causing the polymer chain to grow, and termination with dilute acid results in a carboxylic acid endgroup. The coordination-insertion pathway generates the same alkoxide propagating species as the anionic 1 pathway. Prior to the cleavage of the acyl-oxygen and aluminum-oxygen bonds, a 4-atom coordination between GL and A_1 occurs (Figure 14).

The three mechanisms aforementioned were examined computationally to determine which pathway is more favorable for the ROP of GL (Figure 14). The relative zero of enthalpy corresponds to three free GL monomers and one A_1 initiator (all species in Figure 14 include SMD continuum DMF

solvation). The anionic 1 and coordination-insertion pathways share intermediates **I1–3** and, thus, are shown together; however, the green dashed lines indicate the coordination-insertion pathway only and the blue solid lines indicate the intermediates of the anionic 1 pathway. The anionic 2 pathway is denoted with pink dashed lines. The intermediates correspond to the number of ring-opened repeat units of the growing polymer chain (**I2**: M_n=2). The structures of **CRD1–3** involve the coordination of a GL to the aluminum species with the number of ring-opened repeat units being *n–1* (**CRD2**: M_n=1). Comparing the two types of propagating species, the alkoxide of anionic 1 and coordination-insertion is more favorable than the carboxylate of anionic 2. The alkoxide species is approximately 5 kcal mol^{-1} lower in enthalpy than the carboxylate species in **I1**, increasing by an additional 5 kcal mol^{-1} for each successive intermediate. The evidence for a coordination-insertion pathway is demonstrated by the low energy coordination species **CRD1–3** followed by a low TS barrier. Moreover, the **TS1** species of coordination-insertion is only a 6 kcal mol^{-1} barrier to form **I1** from **CRD1**, further suggesting the probability of the coordination-insertion pathway. While the distinction between anionic 1 and coordination-insertion is rather ambiguous, it is clear that the alkoxide propagating species is more favorable than the carboxylate propagating species of anionic 2.

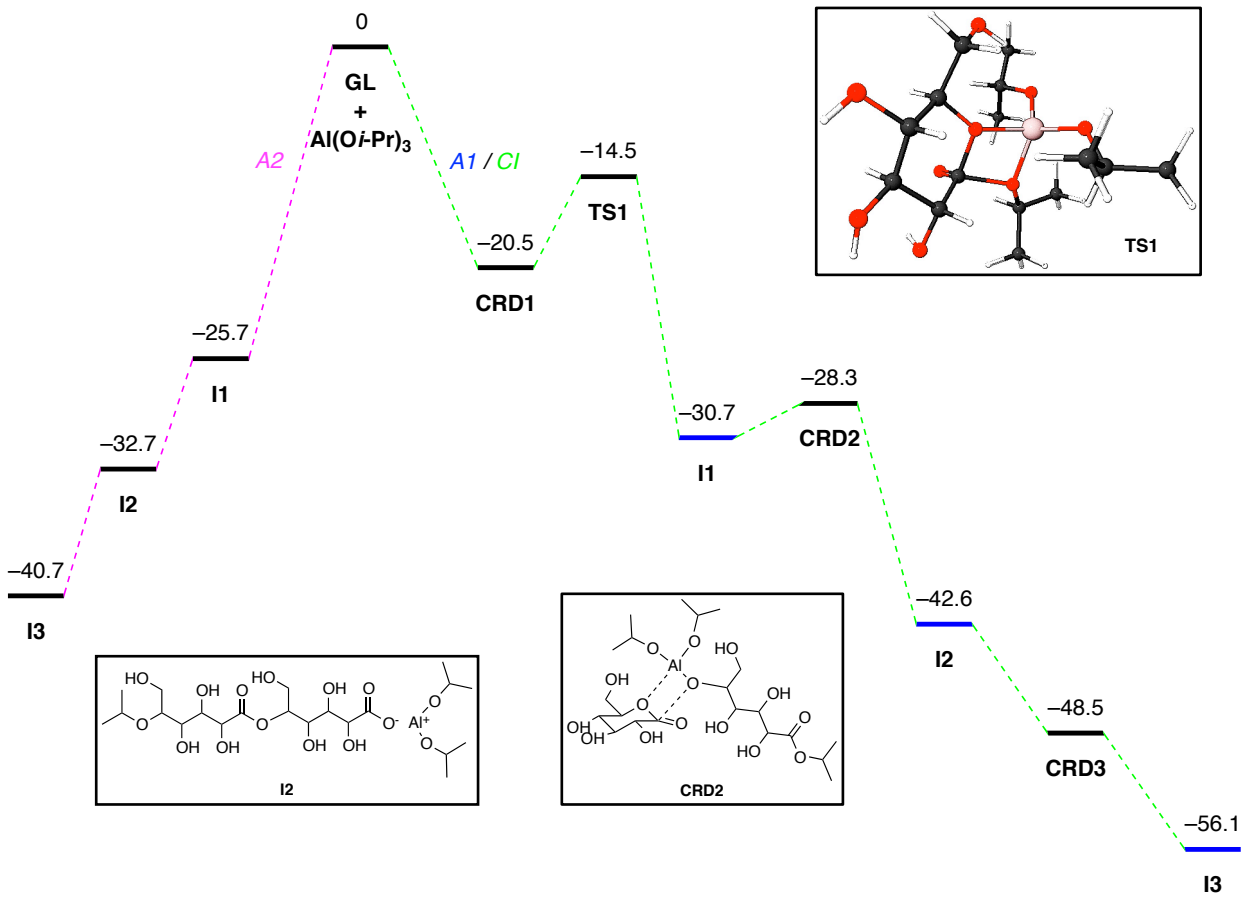

Figure 14. Potential energy surface of GL polymerization initiated by Al(O*i*-Pr)$_3$ monomer, A_1. DFT calculations were performed using M06L/6-31G(d) with density fitting and the SMD solvation model (DMF). All values are of the enthalpies in kcal mol^{-1}. Coordination indicates 4-atom coordination and the overall number of GL molecules in the calculation; the number of coordinated GL molecules is *n* and the number of ring-opened GL molecules is *n–1* (**CRD2**: M_n=1). Each intermediate indicates the number of ring-opened GL molecules (**I2**: M_n=2). The blue solid lines represent the anionic 1 pathway, the pink dashed lines represent the anionic 2 pathway and the green dashed line represent the coordination-insertion pathway. A 3D view of **TS1** is depicted as well as sample intermediate and coordination structures [C = black, O = red, H = white, Al = brown].

The stability of the Al(O*i*-Pr)$_3$ monomer, dimer, trimer and tetramer towards ROP of GL were also examined computationally (Figure 15). Based on experimental ^{1}H NMR kinetic studies, it is believed that A_3 and A_4 exist in equilibrium.[7] Our theoretical calculations support this assertion, demonstrating a large enthalpic gain for each higher order aggregate. Furthermore, the reactivity of the aluminum aggregates was investigated to determine which one would be the most favorable for initiation of ROP. Initial calculations were made with a model system using two simple esters of acetic acid (Scheme 7). This was to determine which aluminum aggregate would favorably cleave the acyl-oxygen bond as well as if the bulkiness of the endgroup had an effect on the reaction. The focus was on the outermost

isopropoxide ligands because they are much more nucleophilic than the oxygen-bridged ligands. One exception arises with A_3, which has an additional free ligand on the central aluminum. In the case of A_3, calculations were performed to determine which ligand was most reactive in the system. The results show that the inner ligand is more reactive than the outer ligands by approximately 5 kcal mol^{-1}; thus, the inner ligand was used for each successive reactivity calculation. Intriguingly, the model system revealed that A_4 was better at cleaving the acyl-oxygen bond than A_3 by 85 and 70 kcal mol^{-1} when R = Me and *t*-Bu, respectively. Since the model system exhibited unexpected results, the formation of **I1** through the anionic 1 pathway was examined for each aggregate (Scheme 8). The most reactive aluminum species was A_2, followed by A_1, A_4 and A_3 (Table 1). Again, A_3 was found to be the least reactive in this system; the reason behind this is not currently understood. One potential cause of this is due to the amount of heteroatoms, high polarity and great complexity of GL as compared to monomers from previous studies of Al(O*i*-Pr)$_3$-initiated ROP. Another potential source of variation is due to solvent effects; DMF is far more polar than common solvents for the aforementioned monomers, which are generally nonpolar.

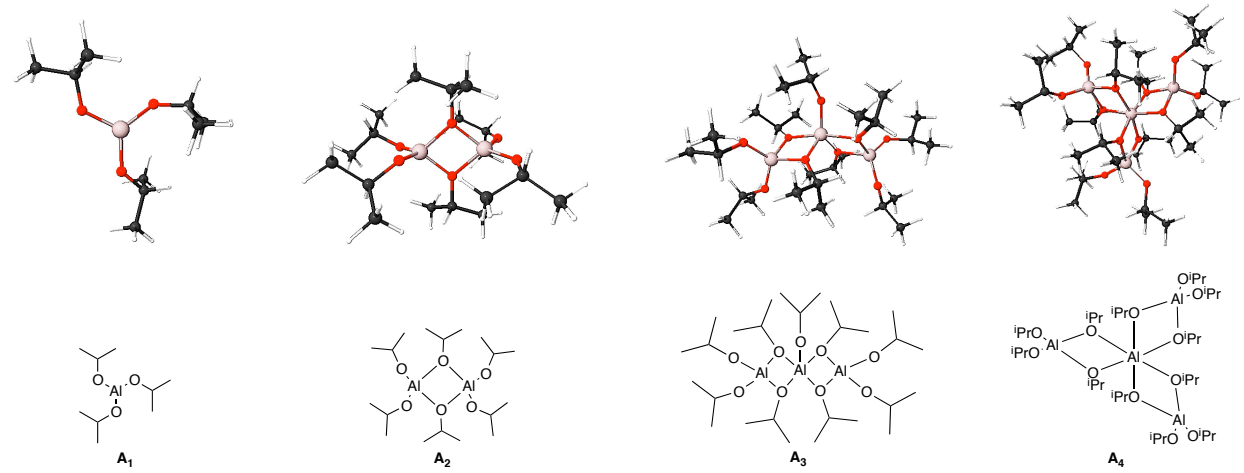

Figure 15. A 3D view of the geometry of the aggregation structures of aluminum isopropoxide [C = black, O = red, H = white, Al = brown]. All values are of the relative free energies in kcal mol^{-1}.

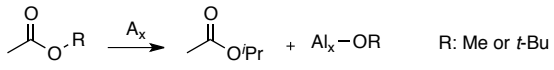

Scheme 7. Model system used for determination of acyl-oxygen cleavage of GL by each aluminum aggregate.

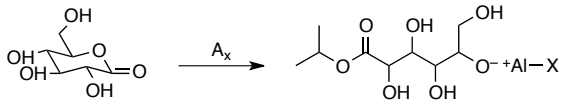

Scheme 8. Formation of **I1** from GL to determine aluminum aggregate reactivity in the actual system of interest.

Table 1. Formation of **I1** through the anionic 1 pathway for each aggregate.

Aggregate	ΔH (kcal mol^{-1})
A_1	–32.72
A_2	–41.16
A_3	–14.01
A_4	–20.40

CONCLUSION

Highly functionalized polymers derived from a renewable feedstock were synthesized. Two approaches were taken and yielded different results. The condensation polymerization of glucose and fructose by metaboric acid and Ti(O*n*-Bu)$_4$ in IL media proved to be unsuccessful. This is likely due to the degradation of the carbohydrate monomers as a result of reaction conditions including high temperature for the removal of formed water and the facilitation of HMF formation by the IL media. The ring-opening polymerization of gluconolactone and acetyl-gluconolactone were initiated by Al(O*i*-Pr)$_3$ in DMF and THF, respectively. NMR and FT-IR spectroscopy provided evidence for the characterization of the renewable polymers. The mechanism and reactivity of Al(O*i*-Pr)$_3$ and its aggregates were also investigated through computational methods. This study suggests that the ROP of GL proceeds via a coordination-insertion mechanism and is initiated by the tetrameric aluminum species. These polymers are excellent candidates for the manufacture of sustainable polymers derived from a fully renewable carbohydrate feedstock.

ACKNOWLEDGMENTS

I would like to thank Dr. Dean Katahira and Dr. Joseph Scanlon for their guidance throughout the course of this study. I would also like to thank Dr. Patrick Willoughby for his helpful insights with experimental support and instrumental analysis. Furthermore, thank you to the Ripon College Chemistry

Department, Ripon College McNair Scholars Program, Midwest Undergraduate Computational Chemistry Consortium (NSF CHE-1039925) and Ripon College Center for Social Responsibility for the opportunity and support to conduct this research. Finally, I would like to thank friends and family for their support and willingness to listen to me ramble about polymers.

REFERENCES

(1) Hillmyer, M. A.; Tolman, W. B. *Acc. Chem. Res.* **2014**, *47*, 2390–2396.
(2) U.S. Environmental Protection Agency. *Municipal Solid Waste*, **2014**, <http://www.epa.gov/epawaste/nonhaz/municipal/>.
(3) Gallagher, J. J.; Hillmyer, M. A.; Reineke, T. M. *Macromolecules* **2014**, *47*, 498–505.
(4) Meng, X.; Matson, J. B.; Edgar, K. J. *Biomacromolecules* **2014**, *15*, 177–187.
(5) Hufendiek, A.; Trouillet, V.; Meier, M. A. R.; Barner-Kowollik, C. *Biomacromolecules* **2014**, *15*, 2563–2572.
(6) Hassan, E. R. E.; Mutelet, F.; Pontvianne, S.; Moïse, J. *Environ. Sci. Technol.* **2013**, *47*, 2809–2816.
(7) Albertsson, A.; Varma, I. K.; *Biomacromolecules* **2003**, *4*, 1466–1486.
(8) Dechy-Cabaret, O.; Martin-Vaca, B.; Bourissou, D. *Chem. Rev.* **2004**, *104*, 6147–6176.
(9) Xavier, N. M.; Rauter, A. P.; Queneau, Y. *Top. Curr. Chem.* **2010**, *295*, 19–62.
(10) Haider, A. F.; Williams, C. K. *J. Polym. Sci. A Polym. Chem.* **2008**, *46*, 2891–2896.
(11) Ding, K.; Miranda, M. O.; Moscato-Goodpaster, B.; Ajellal, N.; Breyfogle, L. E.; Hermes, E. D.; Schaller, C. P.; Roe, S. E.; Cramer, C. J.; Hillmyer, M. A.; Tolman, W. B. *Macromolecules* **2012**, *45*, 5387–5396.
(12) Miranda, M. O.; DePorre, Y.; Vazquez-Lima, H.; Johnson, M. A.; Marell, D. J.; Cramer, C. J.; Tolman, W. B. *Inorg. Chem.* **2013**, *52*, 13692–13701.
(13) Tian, D.; Pubois, P.; Jérôme, R. *Macromolecules* **1997**, *30*, 2575–2581.
(14) Mora, P. T.; Wood, J. W. *J. Am. Chem. Soc.* **1958**, *80*, 685–692.
(15) Zakrzewska, M. E.; Bogel-Łukasik, E.; Bogel-Łukasik, R. *Energy Fuels* **2010**, *24*, 737–745.
(16) Chen, G.; Kim, H.; Kim, E.; Yoon, J. *Eur. Polym. J.* **2006**, *42*, 468–472.
(17) Morgenlie, S. *Acta. Chem. Scand.* **1971**, *25*, 1154–1155.
(18) Indurugalla, D.; Bennet, A. J. *J. Am. Chem. Soc.* **2001**, *123*, 10889–10898.
(19) Nuyken, O.; Pask, S. D. *Polymers* **2013**, *5*, 361–403.
(20) Frisch, M. J.; Trucks, G. W.; Schlegel, H. B.; Scuseria, G. E.; Robb, M. A.; Cheeseman, J. R.; Scalmani, G.; Barone, V.; Mennucci, B.; Petersson, G. A.; Nakatsuji, H.; Caricato, M.; Li, X.; Hratchian, H. P.; Izmaylov, A. F.; Bloino, J.; Zheng, G.; Sonnenberg, J. L.; Hada, M.; Ehara, M.; Toyota, K.; Fukuda, R.; Hasegawa, J.; Ishida, M.; Nakajima, T.; Honda, Y.; Kitao, O.; Nakai, H.; Vreven, T.; Montgomery, J. A.; Peralta, J. E.; Ogliaro, F.; Bearpark, M.; Heyd, J. J.; Brothers, E.; Kudin, K. N.; Staroverov, V. N.; Kobayashi, R.; Normand, J.; Raghavachari, K.; Rendell, A.; Burant, J. C.; Iyengar, S. S.; Tomasi, J.; Cossi, M.; Rega, N.; Millam, J. M.; Klene, M.; Knox, J. E.; Cross, J. B.; Bakken, V.; Adamo, C.; Jaramillo, J.; Gomperts, R.; Stratmann, R. E.; Yazyev, O.; Austin, A. J.; Cammi, R.; Pomelli, C.; Ochterski, J. W.; Martin, R. L.; Morokuma, K.; Zakrzewski, V. G.; Voth, G. A.; Salvador, P.; Dannenberg, J. J.; Dapprich, S.; Daniels, A. D.; Farkas, Ö.; Foresman, J. B.; Ortiz, J. V.; Cioslowski, J.; Fox, D. J. *Gaussian 09, Revision A.02*; Gaussian, Inc.: Wallingford, CT, 2010.
(21) Zhao, Y.; Truhlar, D. G. *J. Chem. Phys.* **2006**, *125*, 194101–194118.
(22) Hehre, W. J.; Random, L.; Schleyer, P. v. R.; Pople, J. A. *Ab Initio Molecular Orbital Theory*; Wiley: New York, 1986.
(23) Cramer, C. J. *Essentials of Computational Chemistry: Theories and Models*, 2nd.; John Wiley & Sons: Chichester, U.K., 2004.
(24) Marenich, A. V.; Cramer, C. J.; Truhlar, D. G. *J. Phys. Chem. B* **2007**, *113*, 6378–6396.
(25) Shao, Y.; Molnar, L. F.; Jung, Y.; Kussmann, J.; Ochsenfeld, C.; Brown, S. T.; Gilbert, A. T. B.; Slipchenko, L. V.; Levchenko, S. V.; O'Neill, D. P.; DiStasio Jr., R. A.; Lochan, R. C.; Wang, T.; Beran, G. J. O.; Besley, N. A.; Herbert, J. M.; Lin, C. Y.; Van Voorhis, T.; Chien, S. H.; Sodt, A.; Steele, R. P.; Rassolov, V. A.; Maslen, P. E.; Korambath, P.P.; Adamson, R. D.; Austin, B.; Baker, J.; Byrd, E. F. C.; Dachsel, H.; Doerksen, R. J.; Dreuw, A.; Dunietz, B. D.; Dutoi, A. D.; Furlani, T. R.; Gwaltney, S. R.; Heyden, A.; Hirata, S.; Hsu, C-P.; Kedziora, G.; Khalliulin, R. Z.; Klunzinger, P.; Lee, A. M.; Lee, M. S.; Liang, W. Z.; Lotan, I.; Nair, N.; Peters, B.; Proynov, E. I.; Pieniazek, P. A.; Rhee, Y. M.; Ritchie, J.; Rosta, E.; Sherrill, C. D.; Simmonett, A. C.; Subotnik, J. E.; Woodcock

III, H. L.; Zhang, W.; Bell, A. T.; Chakraborty, A. K.; Chipman, D. M.; Keil, F. J.; Warshel, A.; Hehre, W. J.; Schaefer, H. F.; Kong, J.; Krylov, A. I.; Gill, P. M. W.; Head-Gordon, M. *Phys. Chem. Chem. Phys.* **2006**, *8*, 3172.
(26) Lewkowski, J. *Arkivoc* **2001**, *1*, 17-54.
(27) Ståhlberg, T.; Fu, N.; Woodley, J. M.; Riisager, A. *Chem. Sus. Chem.* **2011**, *4*, 451–458.

SUPPORTING INFORMATION

Table S1. Enthalpy, free energy, entropy values of GL and Al(O*i*-Pr)$_3$ monomer, dimer, trimer and tetramer.

Compound	H (Hartree)	H (kcal mol^{-1})	rel. ΔG (kcal mol^{-1})	rel. ΔS (cal mol^{-1} K^{-1})
GL	–685.71	–430283.41	–	–
A_1	–823.44	–516712.24	0.00	0.00
A_2	–1647.01	–1033501.39	–58.40	–62.05
A_3	–2470.53	–1550266.49	–91.48	–128.38
A_4	–3294.09	–2067054.24	–148.84	–189.25

Table S2. Enthalpy, free energy, and entropy values of A1 Pathway initiated by A_1.

Compound	H (Hartree)	H (kcal mol^{-1})	rel. ΔG (kcal mol^{-1})	rel. ΔS (cal mol^{-1} K^{-1})
R	–2880.56	–1807562.46	0.00	0.00
I1	–2880.61	–1807593.25	–17.76	–43.68
I2	–2880.64	–1807608.12	–15.68	–100.56
I3	–2880.67	–1807630.87	–21.29	–158.03

Table S3. Enthalpy, free energy, and entropy values of A2 Pathway initiated by A_1.

Compound	H (Hartree)	H (kcal mol^{-1})	rel. ΔG (kcal mol^{-1})	rel. ΔS (cal mol^{-1} K^{-1})
R	–2880.56	–1807562.46	0.00	0.00
I1	–2880.61	–1807591.51	–14.07	–50.23
I2	–2880.63	–1807602.00	–10.33	–97.97
I3	–2880.65	–1807613.66	–8.39	–143.56

Table S4. Enthalpy, free energy, and entropy values of CI Pathway initiated by A_1.

Compound	H (Hartree)	H (kcal mol^{-1})	rel. ΔG (kcal mol^{-1})	rel. ΔS (cal mol^{-1} K^{-1})
R	–2880.56	–1807562.46	0.00	0.00
CRD1	–2880.60	–1807587.01	–8.52	–53.77
TS1	–2880.59	–1807580.86	–1.07	–58.12
I1	–2880.61	–1807593.25	–17.76	–43.68
CRD2	–2880.62	–1807600.76	–6.06	–108.11
I2	–2880.64	–1807608.12	–15.68	–100.56
CRD3	–2880.66	–1807622.30	–15.14	–149.91
I3	–2880.67	–1807630.87	–21.29	–158.03